International Journal of Modern Engineering Research (IJMER)

www.ijmer.com Vol.2, Issue.3, May-June 2012 pp-1440-1448 ISSN: 2249-6645

# Wind Turbine Planetry Gearbox Health Diagnostic Using Varying –Time Meshing Stiffness Variation

Prof. Shawki A. Abouel-seoud, Dr. Eid S. Mohamed

*Faculty of Engineering, Helwan University,*
*Cairo, Egypt*

## ABSTRACT

**In wind turbine planetary gearbox, the ability to identify ring-planet-sun gears meshing stiffness from the real data of vibration responses makes it possible to determine the physical existed planet gear defects which used for severity assessments. There are limitations for vibration based gear diagnostic methods. Vibrations are secondary effects in the sense that they are dynamic responses of a gearbox excited by meshing stiffness and other excitations. The aim of this work is to diagnosis the level of defects (gear tooth crack, gear tooth spalling and gear tooth breakage) in wind turbine gearbox using gears meshing stiffness. Varying-time meshing stiffness is used, where, a technique consists of a nonlinear numerical optimization is applied. The optimization uses a dynamic model of the gears mesh and forms an estimate of both time-varying and frequency-varying mesh stiffness that best corresponds to the given set of vibration data. Multi-hour tests were conducted and recordings were acquired using rotational vibration monitoring, where the optimum meshing stiffness was computed. The optimum meshing stiffness with the recording time were highlighted suggesting critical changes in the operation of the gearbox. The results indicate that if one tooth is defected due to cracks, spalling and breakage to reach the setting maximum level, the maintenance regime will be called despite a new damage is prone in the adjacent tooth to save time and cost.**

**KEYWORDS**: Optimum meshing stiffness, spalling, breakage, crack, optimization, vibration responses, planetary gearbox

## NOMENCLATURE

| | |
|---|---|
| $m_e$ | Equivalent mass of the pinion (sum gear) |
| $K_{me}(t)$ | Equivalent gears time-varying meshing stiffness |
| $C_{me}(t)$ | Equivalent gears time-varying meshing damping |
| $h[k]$ | The filter coefficient. |
| $Y[n]$ | The filter output. |
| $X[n-k]$ | Input data |

## 1- INTRODUCTION

Over the last two decades, problems arising from excessive wear, crack and gear tooth surface pitting in gear transmission systems have been of increasing concern for a variety of gear users. At increased power and high loads, gear wear and fatigue failures are major concerns in wind turbine applications. While regular visual inspections and preventive maintenance can help to reduce the failure rate of gear systems, the cost and downtime required make such programs inefficient and uneconomical. On the other hand, vibration signature analysis methodologies are being developed to examine non-intensively the health and wear of gear transmission systems. Using spectra analysis, the amplitude of the frequency spectrum of the measured vibration signal is obtained and displayed in a continuous manner. However, the spectral analysis technique is difficult to apply in a highly complex system where the large number of spectral lines often makes it difficult to detect significant changes in the spectrum **[1]**.

Several methods have been recently developed to tray to produce an index that, when tracked over time, gives some indication of the health of a gearbox. One of these indices is the time-varying meshing stiffness which can be extracted from the vibration of a gearbox (either calculated or measured). In turn, it gives an accurate account of the state of gears. Gear tooth damage and other defects reduce time-varying meshing stiffness and therefore produce changes (or "modulations" in the amplitude envelope and phase of the tooth mesh vibration **[2]**.

A technique for processing vibration data to quantify the level of damage (crack only) in gear system is shown. The technique consists of a nonlinear numerical optimization. The optimization uses a dynamic model of the gear mesh used in vehicle gearbox and forms an estimate of both time-varying and frequency-varying mesh stiffness that best corresponds to the given set of vibration data **[3, 4]**. The procedure developed in these studies can be applied as a part of either an onboard machine health monitoring system or a health diagnostic system used in the regular maintenance. As the developed methodology is based on the analysis of gearbox vibration under normal operating conditions, no shutdown or special modification of the operating parameter is required during the diagnosis process.

The detection and quantification (which is based on the reduction in tooth stiffness) of damage incurred by spur gear teeth were presented using vibration analysis. Gear tooth damage can be caused by a variety of factors including inadequate lubrication, inappropriate operating conditions or specifications, material insufficiencies, and manufacturing or installation problems. Effective lubrication of gear systems is of critical importance because it prevents direct tooth contact, reduces friction

www.ijmer.com Vol.2, Issue.3, May-June 2012 pp-1440-1448 ISSN: 2249-6645

and vibration levels, removes heat generated in the mesh, and protects the gears from corrosion. When the tooth surfaces are subjected to excessive stress conditions, tooth surface failure may occur. This can cause removal and/or plastic deformation of the contacting tooth surfaces **[5, 6]**. In some cases, surface fatigue cracks occur in plastically deformed regions under excessive contact stress, and these can also be caused by scuffing or wear failure. Once initiated, crack propagation is accelerated by the hydroulicing effect of gear lubricant and tangential tractive force. If surface deterioration is not corrected in the early stages of development, catastrophic tooth failure may result. In general, tooth damage causes a reduction in gear tooth stiffness, and severity of tooth damage can be assessed by considering the reduction in its stiffness. Tooth stiffness is a key parameter in gear dynamics in determination of factors such as load-carrying capacity of gears, dynamic tooth loads, vibration characteristics of geared system, and many works have been carried out to calculate the tooth stiffness and its effects upon those factors for many years **[7]**.

However, the aim of this work is to diagnosis the level of defects (gear tooth crack, gear tooth spalling and gear tooth breakage) in wind turbine gearbox using gears meshing stiffness. Varying-time meshing stiffness is used, where, a technique consists of a nonlinear numerical optimization is applied. The optimization uses a dynamic model of the sun-planet-ring gears mesh and forms an estimate of both time-varying and frequency-varying mesh stiffness that best corresponds to the given set of vibration data.

## 2- GEAR TOOTH DAMAGE DETERMINATION

### 2.1 Background

A damage changes stiffness of the tooth, which, in turn, has an effect on the gear meshing dynamics and actual dynamic load. Therefore, it is necessary to compute the dynamic load after each damage increment on order to obtain an accurate prediction of the residual life. As it is, it is assumed that good gears can only be simulated because all the teeth on the same gear have the same meshing stiffness which is not the case in the presence of a cracked tooth.

### 2.2 Single-Degree-of-Freedom Model

**Figure 1** shows a simple single degree-of-freedom model that will account for residual vibration as well as quantification of element damage in a contact force-closed gear teeth system. The system considered in this task consisted of a small pinion (sun gear) in mesh with a larger gear combination (planet and ring), where the ring gear is fixed to the gearbox structure. The two gear masses connected by a spring and a damper. The larger gear combination (planet and ring) is much heavier than the small pinion; hence, it is assumed to be rigid, so that all relative motion between the two is attributed to the motion of the pinion (sun gear). Then, the equation of motion of the pinion (sun gear) takes the form.

$$\sum F = m\ddot{X} \quad (1)$$

$$m_e\ddot{X} + C_{me}(t)\dot{X} + K_{me}(t) * X = 0 \quad (2)$$

$$C_{me}(t) = \mu K_{me}(t) \quad (3)$$

$$m_e * \ddot{X} + \mu K_{me}(t) * \dot{X} + K_{me}(t) * X = 0 \quad (4)$$

$$m_e * \ddot{X} + K_{me}(t) * (\mu\dot{X} + X) = 0 \quad (5)$$

Where*:*

$m_e$ = Equivalent mass of the pinion (sum gear)
= $[(m_s*3m_p) / (m_s+3m_p)]$

$K_{me}(t)$ = Equivalent gears time-varying meshing stiffness

$C_{me}(t)$ = Equivalent gears time-varying meshing damping

$\mu = 3.99 * 10^{-3}(s)$ **[8]**.

### 2.3 Optimization Technique

The unknown time-varying meshing stiffness is assumed to be periodic and therefore can be represented by a truncated Fourier series, which is then embedded into the lumped parameter model. For a healthy gear that has regularly spaced identical teeth, the time-varying meshing stiffness is largely repeated from one tooth to the next with the fundamental frequency of tooth meshing. On the other hand, a faulty gear tooth gives a meshing pattern that is repeated largely once a revolution. The optimization technique is used to process vibration data to quantify the level of damage in a gear transmission system. The optimization uses a dynamic model of the gear mesh and forms an estimate of the time-varying mesh stiffness that best correspond to the given set of vibration data. An analysis of this relationship demonstrates that the perturbation of the stiffness function from the nominal profile can be used to quantify the level of crack damage. Referring to equation (5), the meshing stiffness is not constant but is nominally a periodic function of the time, with each period corresponding to one tooth pass. It has been found in experiments on gearbox vibrations that the gear meshing stiffness changes with the damages of the gear teeth. Such changes in the gear meshing stiffness inevitably lead to changes in the vibration signatures of the mechanical system. The objective of the optimization technique developed in this task is to reconstruct the true stiffness profile for a damaged gear tooth from the measured vibration. That is, the objective is to determine the function $K_{me}(t)$ that would result in the measured vibration according to the system model in **Fig. 1**.

www.ijmer.com Vol.2, Issue.3, May-June 2012 pp-1440-1448 ISSN: 2249-6645

**2.4 The Optimization Algorithm**

**A) Background**

Basically, digital filters are used to modify the characteristic of signals in time and frequency domain and have been recognized as primary digital signal processing (DSP). In DSP, the design methods were mainly focused in multiplier-based architectures to implement the multiply-and-accumulate (MAC) blocks that constitute the central piece in finite impulse response (FIR) filters and several functions. Several multipliers-less schemes had been proposed. These methods can be classified in two categories according to how they manipulate the filter coefficients for the multiply operation. The first type of multiplier-less technique is the conversion-based approach, in which the coefficients are transformed to other numeric representations whose hardware implementation or manipulation is more efficient than the traditional binary representation. Example of such techniques are the Canonic Sign Digit (CSD) method, in which coefficients are represented by a combination of powers of two in such a way that multiplication can be simply implemented with adder/subtractors and shifters, and the Dempster-Mcleod method, which similarly involves the representation of filter coefficients with powers of two but in this case arranging partial results in cascade to introduce further savings in the usage of adders. The second type of multiplier-less method involves use of memories (RAMs, ROMs) or Look-Up Tables (LUTs) to store pre-computed values of coefficient operations. These memory-based methods involve Constant Coefficient Multiplier method and the very-well known Distributed Arithmetic method as examples. Distributed Arithmetic (DA) algorithm appeared as a very efficient solution especially suited for LUT-based FPGA architectures. For this reason, the FIR filter is used in this task to optimize the predicted time and frequency-domain meshing stiffness, where the multiplier-less method is used. The multiplier-less method contains look-up tables (LUTs) to store pre-computed values of coefficient operations. These memory-based methods involve constant coefficient multiplier method and the very-well known distributed arithmetic algorithm (DA) **[9, 10]**.

**B) Finite impulse response (FIR) filter**

Digital finite impulse response (FIR) filters have been used in signal processing as ghost cancellation and channel equalization. FIR filtering of which the output is described in Equation (6) is realized by a large number of adders, multipliers and delay elements.

$$Y[n] = \sum_{k=0}^{N-1} h[k].X[n-k] \qquad (6)$$

Where $Y[n]$ is the filter output, $X[n-k]$ is input data, and $h[k]$is the filter coefficient. Direct form of a finite word truncating is the optimum infinite precision coefficients determined by McClellan and Parks algorithm **[11].** Due to the enormous occupied area of FIR filters with a large number of taps, hardware-reusing architectures such as time-multiplexing architectures and a distributed arithmetic (DA) approach based on bit-serial access, have been widely adopted for implementation. Canonical Signed-Digit (CSD) coefficient representation has also been used by many researchers for designing multiplier-less high speed FIR filters. Canonical Signed Digit encoding is used for coefficients to minimize the number of additions. In many signal processing and communication applications such as FIR filters, video and image processing, a multiplication with constants e.g. filter coefficients have to be performed. Therefore, the use of multiplier-less techniques is inspired to avoid the need of establishing an expensive general purpose multiplier e.g. on the FPGA and instead computing constant multiplications using table lookups and additions.

**C) Distributed arithmetic (DA)**

An alternative approach is the DA technique which is well known method to save resources. However, using this approach, the filter can be implemented in bit serial or parallel mode to trade bandwidth for area utilization. The input variable in equation (6) can be represented in its weighted format as in equation (7).

$$x_k = -x_{n,k-1} + \sum_{m=0}^{k-1} {}^{2-m}_{x_n,k-1-m} \qquad (7)$$

Using equation (7) in (6) and after some mathematical manipulations the filter output given in equation (6) can be written as in equation (8).

$$Y = \sum_{m=0}^{k-1} \sum_{k=0}^{k-1} Z^{2-m}_{k-1-m} \qquad (8)$$

Implementing equation (8) in bit serial DA basic **structure [12]** will result in constructing lookup table (LUT) of size 2m (m is the number of input variables, e.g. filter coefficients). This is the major drawback of the basic DA architecture which made it sometimes impractical for designing high order FIR digital filters. In this problem has been overcome by proposing a new architecture for the DALUT so that its size is independent of the number of input variables or filter coefficient.

**D) Pulse shaping**

In any transmission system, where pulses are transmitted and ultimately detected by the receiver, the goal is to sample the received signal at optimal points in the pulse interval so that the probability of an accurate binary decision is maximized. This implies that the fundamental shapes of the pulses be such that they do not interfere with one another at the optimal point i.e. have zero value at sampling points. In addition, the pulse amplitude must decay rapidly outside the pulse interval. In real systems, it is proved that the quicker a pulse decays outside its interval, the less likely it allow timing jitter to introduce errors when sampling adjacent pulse **[13].**

**E) Algorithm analysis**

The algorithm analysis starts with obtaining the filter coefficients based on desired specifications. Using the round function in MATLAB these coefficients are rounded to the nearest integer after being multiplied with a constant

www.ijmer.com Vol.2, Issue.3, May-June 2012 pp-1440-1448 ISSN: 2249-6645

integer value. Finally, a block diagram for the DA implementation of a FIR filter is shown in **Fig. 2 [14]**.

## 3. EXPERIMENTAL METHODOLOGY

The establishment of the experimental methodology and the accelerometers positions are presented in detailed in **Ref. [15]**, where the measuring of rotational response has been evaluated by using a pair of matched accelerometers placed a short distance apart on the gearbox's structure. Tests were conducted in order to calibrate the sensor configuration and insure the reaptability of the recordings and the proper operation with minimum noise of the system as well as the various cables and connections. . **Fig. 3** shows photograph of test layout, while **Fig. 4** shows the accelerometers postions. Defects with their dimensions have been artificial made in the wind turbine gearbox planet tooth (crack, spalling and breakage) are presented in **Fig. 5.** In terms of various parameters evolution during the test; from a representative test on the planetary gearbox system with different damages will be presented. The defects were made artificially with wire electrical discharge machining (EDM) and chemical electrode on the gearbox to create a stress concentration which eventually led to a propagating fault. This type of test was preferred in order to have the opportunity to monitor bath defects modes, i.e., the natural fault propagation.

Two Bruel & Kjaer accelerometers were used for the rotational vibration monitoring both mounted upon the gearbox case, one in each side-axis. The signal was lowpass filtered at 6.0 kHz through a filter, in order to aliasing distorsion and retain waveform integraty as much as possible. A number of 2048 samples have been acquired in the experimentls corresponding to a time history length of 1.0 s. B&K portable multi-channel PULSE type 3560-B-X05 analyser is used. The B&K PULSE labshop with the measurement software type 7700 is used to analyse the results, while the speed is measured by photo electric probe. Recordings were carried out at constant speed conditions and closed windows. The output speed range is 40 rpm and the torque load is 40 Nm. For each defect, recordings every 60.0 min were acquired and a total of 7 recordings (~ 6.0 h of test duration) were resulted until the termination of the test.

## 4. RESULTS AND DISCUSSION

### 4.1 Diagnostic Results and Discussion

**a) Healthy gearbox**

In healthy gearbox, **Fig. 6** shows the time-domain of mean vibration displacement, velocity and acceleration responses for speed 40 rpm and 40 Nm**. Fig. 7** shows the comparison between the computed time-varying nominal meshing stiffness based on equation (5) and optimum meshing stiffness based on equation (8) at speed 40 rpm. Note that the frequency range is up to 6000 Hz (**Fig. 7- b**), where the highest stiffness levels are observed to be up to 1000 Hz (**Fig. 7-c**), while the levels of the remaining frequency are lower and almost constant. However, the frequency's range up to 1000 Hz which shown in **Fig. 7-c** is used for the diagnostic purpose.

**b) Cracked planet gear**

**Figure 8** shows the comparison between optimum meshing stiffness in healthy gearbox and cracked planet gear at speed 40 rpm and 40 Nm in terms of frequency-domain (1000Hz). The effect of irregular optimum meshing stiffness associated with a cracked planet gear tooth is filtered by the gearbox dynamics and contaminated by other vibrations. It is clearly seen from the figure that the optimal meshing stiffness for the cracked planet gear is lower than that for the healthy gearbox particularly at low frequency up to 500 Hz. This is important information for fault detection and severity assessment. Samples for the RMS averages of optimum meshing stiffness at different testing time up to 6.0 h is shown in **Fig. 9**. To assist the more accurate observation of this parameter evaluation during the range of testing time possess diagnostic value as they can be used to define and characterize critical changes of the gears faults accumulation and evaluation. On the other hand, it can be observed that the RMS value decreases as the testing time is increased, where the planet gear tooth crack can make the tooth lose instantaneous loading capacity and consequently work and torque transfer ability. This can be an effective way to carry out the predictive maintenance regime and consequently to save money and look promising.

**c) Spalling planet gear**

**Figure 10** shows the comparison between optimum meshing stiffness in healthy gearbox and spalling planet gear at speed 40 rpm and 40 Nm in terms of frequency-domain (1000Hz). The effect of irregular optimum meshing stiffness associated with a spalling planet gear tooth is filtered by the gearbox dynamics and contaminated by other vibrations. It is clearly seen from the figures that the optimal meshing stiffness for the spalling planet gear is lower than that for the healthy gearbox particularly at low frequency up to 500 Hz. This is important information for fault detection and severity assessment. Samples for the RMS averages of optimum meshing stiffness at different testing time up to 6.0 h is shown in **Fig. 11**. To assist the more accurate observation of this parameter evaluation during the range of testing time possess diagnostic value as they can be used to define and characterize critical changes of the gears damage accumulation and evaluation. The correct detection and diagnosis of a tooth spalling is very important in practical diagnosis because spalling may just result in some noise and extraneous dynamic response. On the other hand, it can be observed that the RMS value decreases as the testing time is increased. This can be an effective way to carry out the predictive maintenance regime and consequently to save money and look promising.

**d) Breakage planet gear**

**Figure 12** shows the comparison between optimum meshing stiffness in healthy gearbox and breakage planet gear at speed 40 rpm and 40 in terms of frequency-domain

www.ijmer.com Vol.2, Issue.3, May-June 2012 pp-1440-1448 ISSN: 2249-6645

(1000Hz). The effect of irregular optimum meshing stiffness associated with a breakage planet gear tooth is filtered by the gearbox dynamics and contaminated by other vibrations. It is clearly seen from the figures that the optimal meshing stiffness for the breakage planet gear is lower than that for the healthy gearbox particularly at low frequency up to 500Hz. This is important information for fault detection and assessment. Samples for the RMS averages of optimum meshing stiffness at different testing time up to 6.0 h are shown in **Fig. 13**. To assist the more accurate observation of this parameter evaluation during the range of testing time possess diagnostic value as they can be used to define and characterize critical changes of the gears damage accumulation and evaluation. The correct detection and diagnosis of a tooth breakage is very important in practical diagnosis because breakage may just result in some noise and extraneous dynamic response. On the other hand, a reduction in the optimum meshing stiffness is observed. This reduction is more accentuated when the testing time increases. This is explained by the fact that when the breakage affects the whole height of the tooth. This can be an effective way to carry out the predictive maintenance regime and consequently to save money and look promising.

**4.2 Planet gear damages severity assessment**

In terms of RMS optimum meshing stiffness**, Fig. 14** depicts planet gear tooth faults (crack, spalling and breakage) severity assessment which has been achieved by the developed the experimental technique at speed 40 rpm and 40 Nm. The testing time is being 0.0 h. The figure indicates that gear breakage posses the highest RMS value followed by gear spalling with gear crack has least RMS. This can help to identify which type of faults can be detected**.** On the other hand, **Table 1** tabulates in percentage of the change of RMS optimum meshing stiffness at testing time of 0.0 h from that for healthy gearbox (*CFHL*) at speed 40 rpm and 40 Nm based on the following equation:

$$CFHL,(\%)=\frac{(RMS)_{Healthy}-(RMS)_{Faulty}}{(RMS)_{Healthy}} \qquad (9)$$

Where

$(RMS)_{Healthy}$ = RMS value for healthy condition

$(RMS)_{Faulty}$ = RMS value for faulty condition

The values are 47.15% (gear breakage), 40.26% (gear spalling) and 30.46% (gear crack). This information can help for diagnostic regime. It has been shown that the fault on gear teeth can be detected at its early stages, and symptoms of defect on vibration is not primarily caused by the reduction in tooth stiffness (which is the case for the detection of a localized tooth defect), but mainly due to the deviations in tooth shape from the true involute profile. The results have revealed that tooth surface fault causes an approximately linear reduction in gear tooth stiffness with time.

## 5. CONCLUSIONS

1- The ability to identify ring-planet-sun gears meshing stiffness from the real data of vibration responses makes it possible to determine the physical existed planet gear damages which used for severity assessments. By using the proposed technique in the real time applications, if one tooth is damaged due to cracks, spalling and breakage to reach the setting maximum level, the maintenance regime will be called despite a new fault is prone in the adjacent tooth to save time and cost.

2- The optimization technique developed in this work provides a very reasonable estimate of the meshing stiffness change due to planet gear fault, which can be related to the state of the gear. Moreover, for more accurate evaluation of the system mesh stiffness, the optimization technique presented needs to be developed.

3- Multi-hour tests were conducted and recordings were acquired using transilational vibration monitoring, where the optimum meshing stiffness was computed, where the optimum meshing stiffness with the recording testing time were highlighted suggesting critical changes in the operation of the gearbox.

4- From this investigation, the gearbox components faults severity assessment has indicated that the values are 30.46% (planet gear crack), 40.26%% (planet gear spalling) and 47.15%% (planet gear breakage). Moreover, the symptoms of fault on vibration is not primarily caused by the reduction components stiffness (which is the case for the detection of a localized fault), but mainly due to the deviations in component shape from the true component shape.

## 6. ACKNOWLEDGEMENTS

The authors acknowledge the support of Science and Technology Development Fund (STDF), Egypt, through the awarded grant No. ID 1484, on monitoring of wind turbine gearbox. The authors would like to thank University of Helwan, which made this study possible.

## REFERENCES

1 Choy, F. K., Polyshchuk, V., Zakrajsek, J. J., Handschuh, R. F. and Townsendi, D. P. " Analysis of the effects of surface pitting and wear on the vibration of a gear transmission system "Tribology International Vol. 29, No. 1, pp. 71-83, 1996.

2 Cai, Y. "Simulation on the rotational vibration of helical gears in consideration of tooth separation phenomenon ( A new stiffness function of helical involutes tooth pair)" ASME, Journal of Mechanical Design, Vol. 177, pp. 460-469, 1995.

3 Choy, F. K., Villette, R. J., Polyshchuk, V. and braun, M. J. " Quantification of gear tooth damage by optimal tracking of vibration signatures" Sixth International Symposium on Transport Phenomena and Dynamics of Rotation Machinery, NASA Technical Memorandum 107100, Feb. 25-29, 1996.

4 Abouel-seoud, S. A., Hmmmad, N., Abdel-halim, N. Abdel-hady, M. amd Mohamed, E. S. " The importance of vehicle gear tooth meshing stiffness in gear tooth Damage quantification" SAE Paper No. 2008-01-2631, 2008.
5 Lin, J. and Parker, R. G. "Planetary gear parametric instability caused by mesh stiffness variation" Journal of Sound and Vibration (2002) 249(1), 129}145, 2002.
6 Stewart RM. "Through-life monitoring of transmission system" Proceedings of the First International Conference on Gearbox Noise, Vibration, and Diagnostics, London: Institute of Mechanical Engineers, pp. 135–40, 1990.
7 Yesilyurta, l., Gub, F. and Ballc,A. D. "Gear tooth stiffness reduction measurement using modal analysis and its use in wear fault severity assessment of spur gears" NDT&E International 36, pp. 357–372, 2003.
8 Bartelmus, W. "Mathematical modelling and computer simulations as an aid to gearbox diagnostics" Mechanical Systems and Signal Processing 15 (5), pp. 855–871, 2001.
9 Eshtawie, M. A. and Othman, M. B. "An Algorithm Proposed for FIR Filter Coefficients Representation" World Academy of Science, Engineering and Technology 26, 2007.
10 Vigneswarn, T. and Reddy, P. S." Design of Digital FIR Filter Based on DDA algorithm" Journal of Applied Science, 2007.
11 Pal, N. S., Singh, H. P., Sarin, R.K. and Singh, S. "Implementation of High Speed FIR Filter using Serial and Parallel Distributed Arithmetic Algorithm" International Journal of Computer Applications (0975 – 8887), Volume 25– No.7, July, 2011.
12 Eshtawie M. A. and Othman, M. B. " On-Line DA-LUT Architecture for High- Speed High-Order Digital FIR Filters," paper status is published in the tenth IEEE international conference on communication systems (IEEE ICCS 2006), 30-1 Nov 2006.
13 Eshtawie, M. A. and Othman, M. B."An Algorithm Proposed For FIR Filter Coefficients Representation" International Journal of Mathematics and computer Sciences, pp24-30, 2008.
14 Proakis, J. G., Salehi, M. and Bauch, G. "Contemporary Communication Systems using MATLAB. Brooks/Cole, 2004.
15 Abouel-seoud, S., El-morsy, M. and Saad, A."A Laboratory Apparatus for Investigation of Vibration Performance of Wind Turbine Planetary Gearbox" Journal of Recent Research, Vol. 3, Issue 11, 2011.

| S/No. | Speed, rpm | Torque, Nm | Gear crack | Gear Spalling | Gear Breakage |
|---|---|---|---|---|---|
| 1 | 40 | 40 | 30.46 | 40.26 | 47.15 |

**Table 1** Change from the healthy gearbox (%)

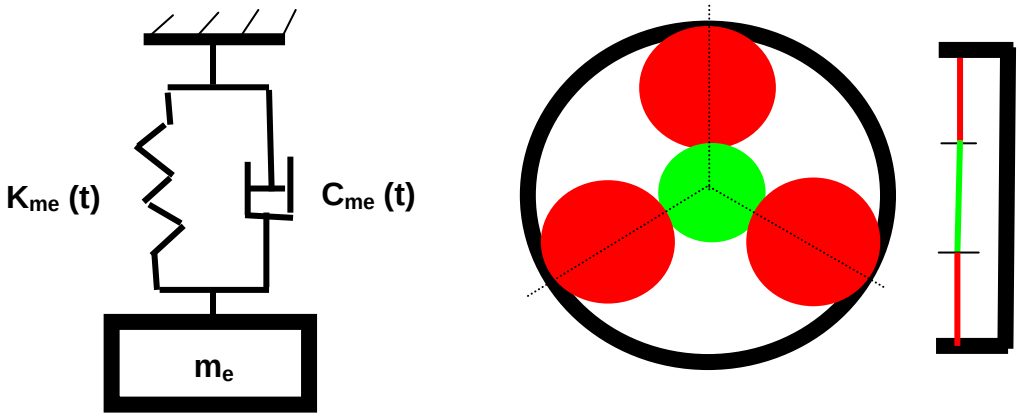


**Fig. 1** Single-degree-of-freedom model

www.ijmer.com Vol.2, Issue.3, May-June 2012 pp-1440-1448 ISSN: 2249-6645

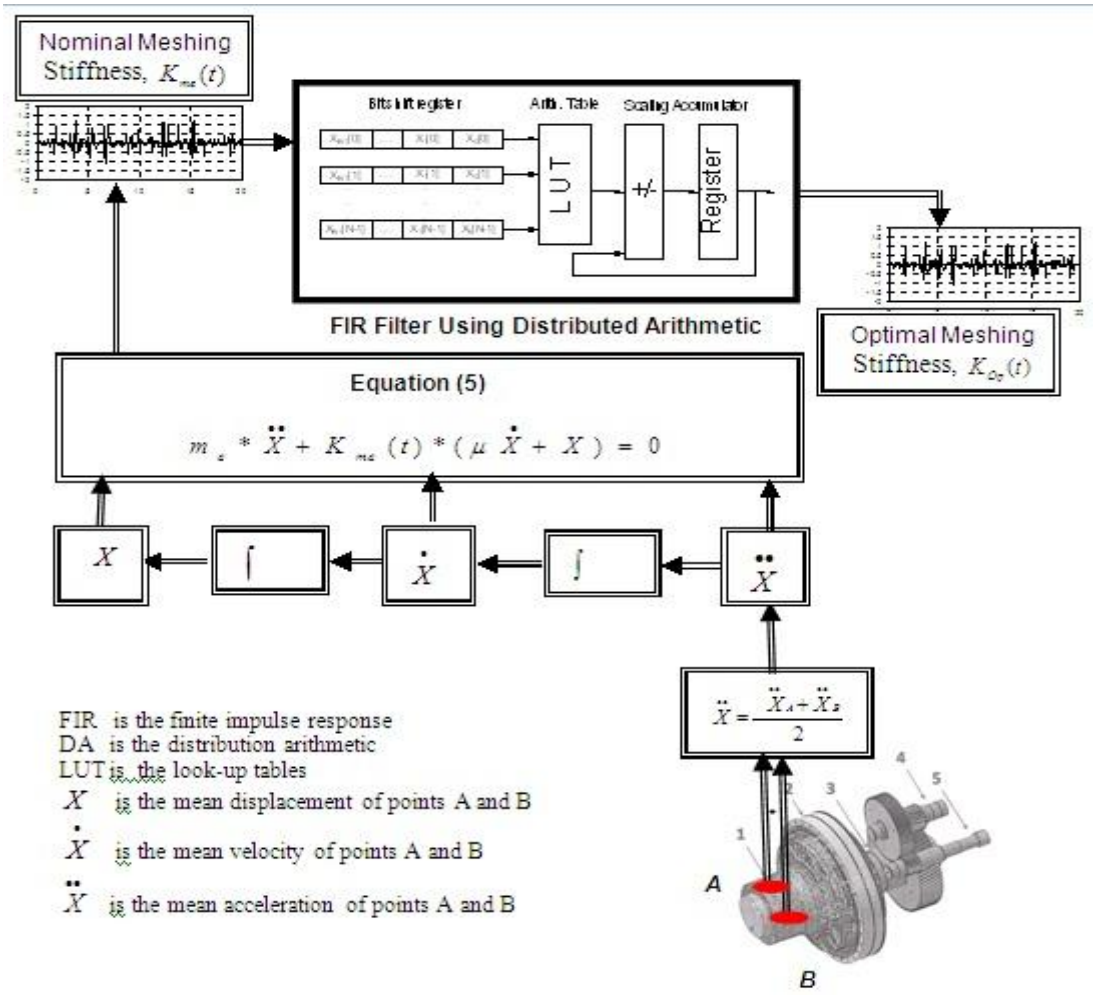


**Fig. 2** Block Diagram for the sequence of optimum meshing stiffness estimation

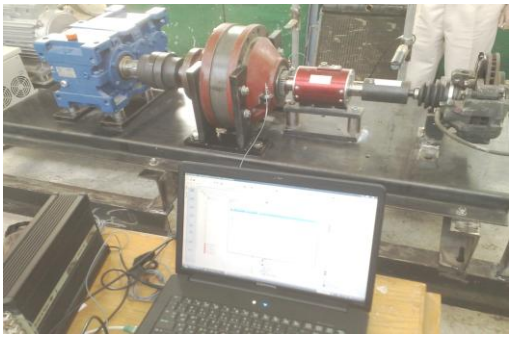

**Fig. 3** Photograph of the layout of the test rig

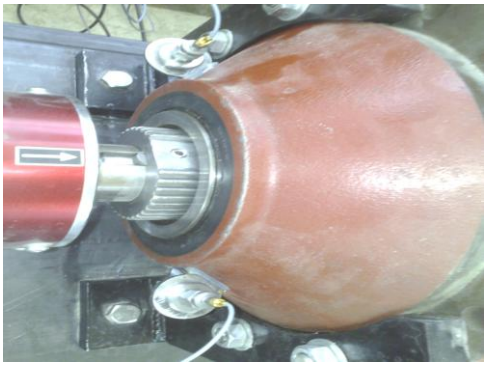

**Fig. 4** Accelerometers positions


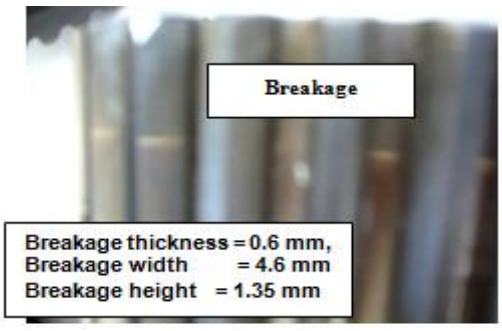

www.ijmer.com Vol.2, Issue.3, May-June 2012 pp-1440-1448 ISSN: 2249-6645

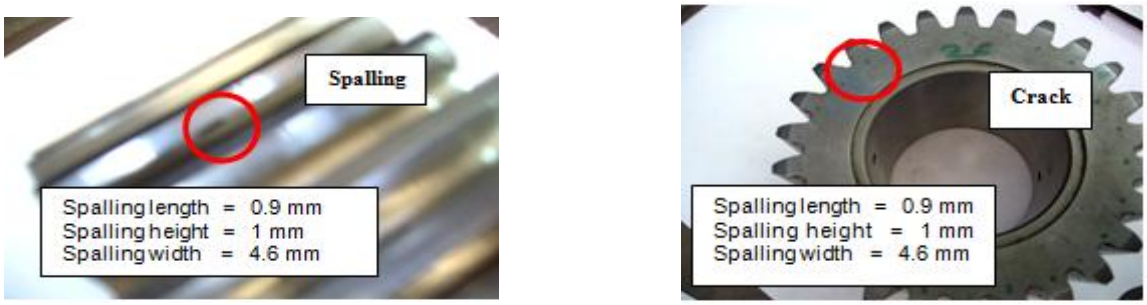


**Fig. 5** Wind turbine planetary gearbox planet gear tooth faults

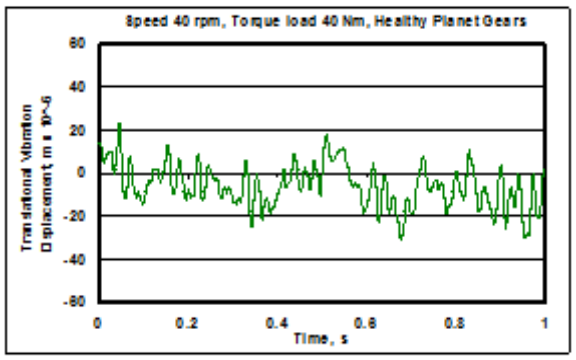


**a)** Mean vibration displacement

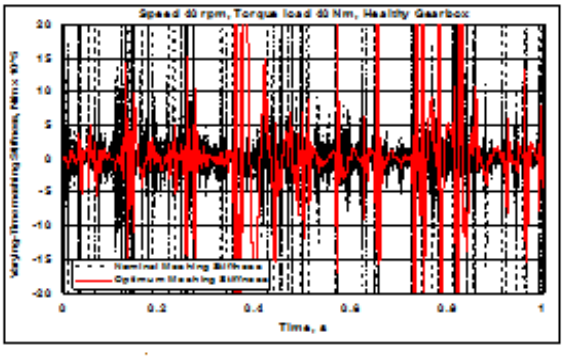


**a)** Time domain signals

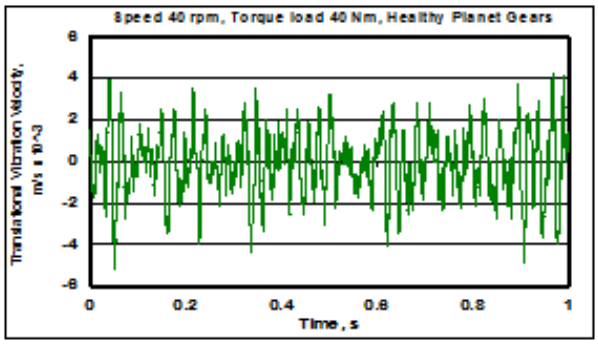


**b)** Mean vibration velocity

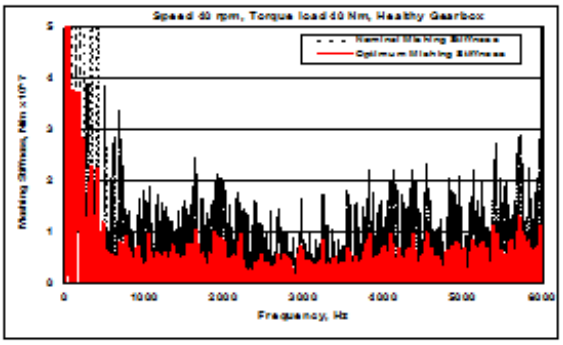


**b)** Frequency-domain (6000 Hz)

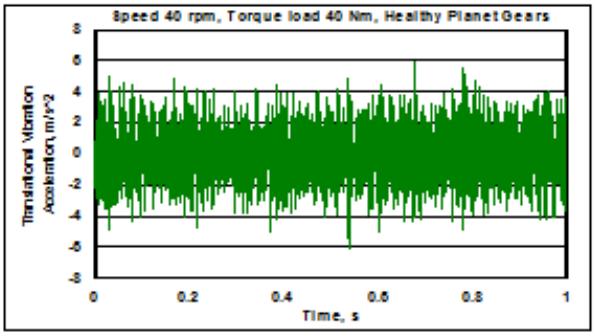


**c)** Mean vibration acceleration

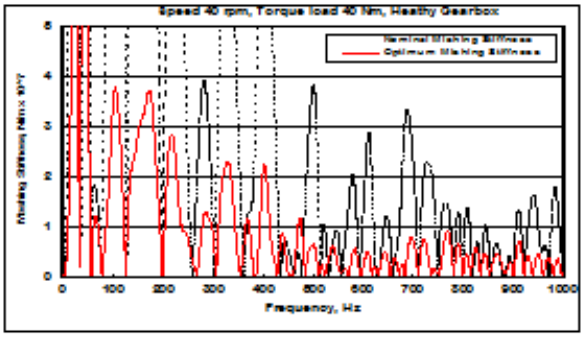


**c)** Frequency-domain (1000 Hz)

**Fig. 6** Vibration responses at 40 rpm, 40 Nm (Healthy gearbox)

**Fig. 7** Meshing stiffness at 40 rpm, torque 40 Nm (Healthy gearbox)

www.ijmer.com Vol.2, Issue.3, May-June 2012 pp-1440-1448 ISSN: 2249-6645

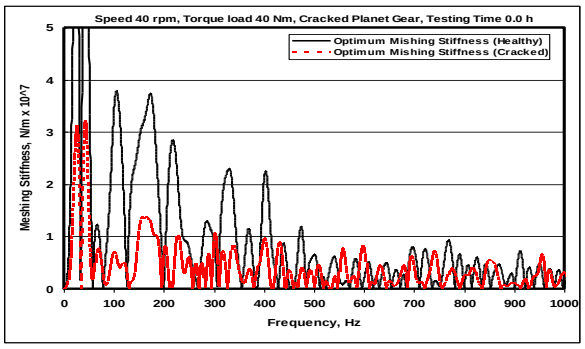


**Fig. 8** Optimum meshing stiffness at 40 rpm, 40 Nm (Cracked Planet Gear)

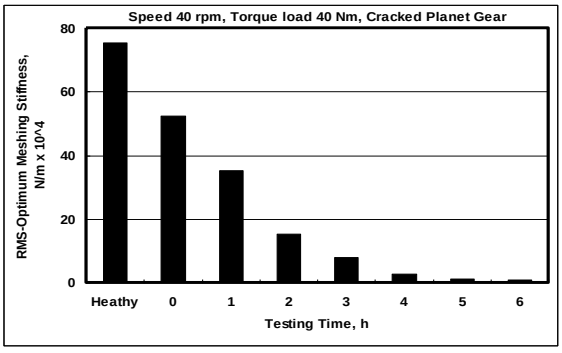


**Fig. 9** RMS-optimum meshing stiffness at 40 rpm 40 Nm (Cracked Planet Gear)

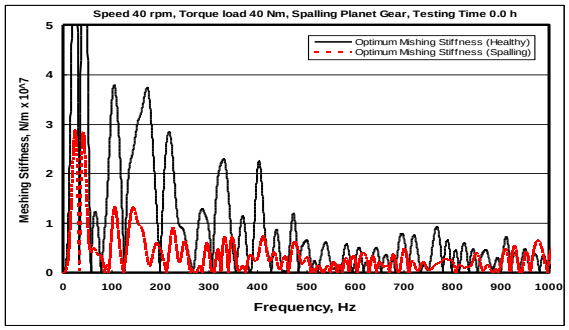


**Fig. 10** Optimum meshing stiffness at 40 rpm, 40 Nm (Spalling Planet Gear)

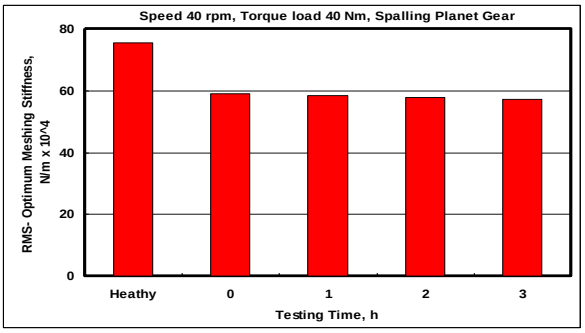


**Fig. 11** RMS-optimum meshing stiffness at 40 rpm 40 Nm (Spalling Planet Gear)

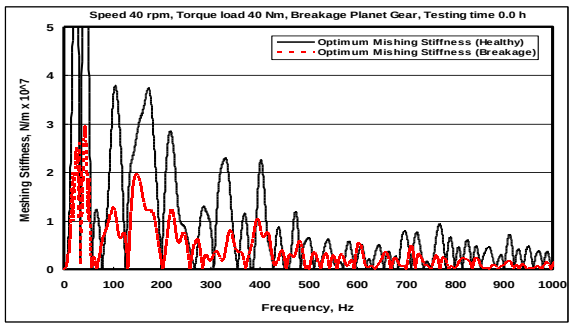


**Fig. 12** Optimum meshing stiffness at 40 rpm, 40 Nm (Breakage Planet Gear)

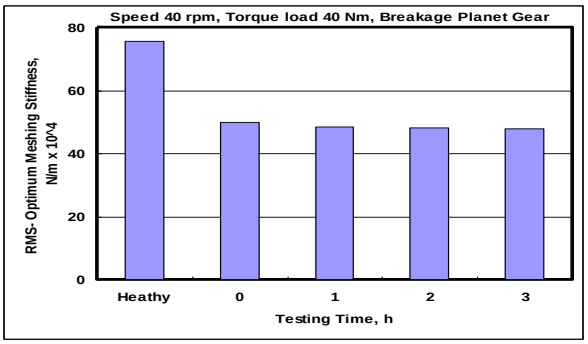


**Fig. 13** RMS-optimum meshing stiffness at 40 rpm 40 Nm (Breakage Planet Gear)

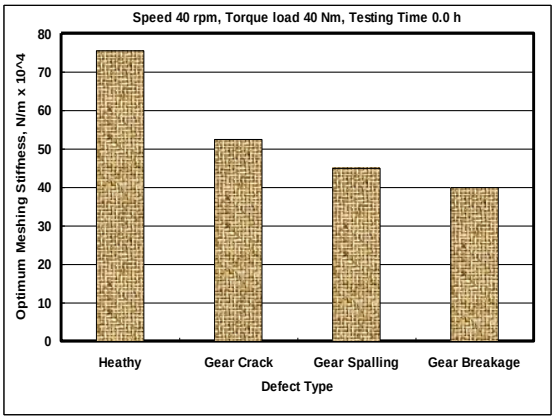


**Fig. 14** RMS-optimum meshing stiffness at 40 rpm 40 Nm